Mathematical and Computational Applications

MDPI

Article

A New Fractional Boundary Element Model for the 3D Thermal Stress Wave Propagation Problems in Anisotropic Materials

Mohamed Abdelsabour Fahmy [1,2,*] and Moncef Toujani [1]

[1] Department of Mathematics, Adham University College, Umm Al-Qura University, Adham, Makkah 28653, Saudi Arabia; aatoujani@uqu.edu.sa
[2] Faculty of Computers and Informatics, Suez Canal University, New Campus, Ismailia 41522, Egypt
* Correspondence: maselim@uqu.edu.sa; Tel.: +966-537930306

Abstract: The primary purpose of this work is to provide a new fractional boundary element method (BEM) formulation to solve thermal stress wave propagation problems in anisotropic materials. In the Laplace domain, the fundamental solutions to the governing equations can be identified. Then, the boundary integral equations are constructed. The Caputo fractional time derivative was used in the formulation of the considered heat conduction equation. The three-block splitting (TBS) iteration approach was used to solve the resulting BEM linear systems, resulting in fewer iterations and less CPU time. The new TBS iteration method converges rapidly and does not involve complicated computations; it performs better than the two-dimensional double successive projection method (2D-DSPM) and modified symmetric successive overrelaxation (MSSOR) for solving the resultant BEM linear system. We only studied a special case of our model to compare our findings to those of other articles in the literature. Because the BEM results are so consistent with the finite element method (FEM) findings, the numerical results demonstrate the validity, accuracy, and efficiency of our proposed BEM formulation for solving three-dimensional thermal stress wave propagation problems in anisotropic materials.

Keywords: boundary element method; fractional order; three-dimensional; thermal stress wave propagation; anisotropic materials

check for updates

Academic Editor: Nicholas Fantuzzi

Received: 6 December 2024
Revised: 1 January 2025
Accepted: 7 January 2025
Published: 8 January 2025

Citation: Fahmy, M.A.; Toujani, M. A New Fractional Boundary Element Model for the 3D Thermal Stress Wave Propagation Problems in Anisotropic Materials. *Math. Comput. Appl.* **2025**, *30*, 6. https://doi.org/10.3390/mca30010006

Copyright: © 2025 by the authors. Licensee MDPI, Basel, Switzerland. This article is an open access article distributed under the terms and conditions of the Creative Commons Attribution (CC BY) license (https://creativecommons.org/licenses/by/4.0/).

1. Introduction

Within the discipline of continuum mechanics, thermoelasticity studies the relationship between mechanical memory and thermodynamics in the behavior of solid bodies. There are various options for doing this. The most general method is to try to put thermodynamic constraints on the constitutive equations, with deformation and temperature as dependent variables [1–3]. In some materials, these constraints are so specific that, among the infinite ways of coupling mechanics and thermodynamics, certain closed sets of equations can be obtained that characterize the unknown driving forces of the coupled field. The most typical sets of linked equations appear to be very simplified versions of what can be obtained using a more generic approach [4]. However, when a non-quadratic elastic energy function is considered, the simplifying feature required to distinguish one theory from others may not always be reduced to the property of meeting a set of equilibrium equations and a temperature equation [5,6].

Fractional calculus is the study of the properties and results of the derivative of a function of order a. It provides tools to understand phenomena and processes that evolve in time in a more accurate way than those offered by classical integral and differential calculus, considering long memories in their internal evolution [7,8]. Moreover, fractional calculus is

naturally used to model processes with unique and non-local effects, which are considered highly complex. Indeed, phenomena described by models based on non-integer order integrals and derivatives have attracted the attention of the scientific community and have been applied in several areas not only as mathematical models but also as theoretical tools for the study of other physical phenomena [9–11]. The rapid development of computational and theoretical techniques to efficiently deal with mathematical models based on fractional calculus, as well as the success of these models in solving mathematical problems, has naturally motivated several scientific researchers to investigate the potential of these models in solving various engineering problems, with positive and significant complex effects. Consequently, fractional calculus models began to spread into distinct traditional fields of engineering like control and power systems, becoming a major topic of investigation in all other fields. Fractional calculus is undoubtedly a very valuable tool for the study of complex media and has a considerable impact in many different fields, both theoretical and experimental. Nevertheless, the physico-mathematical aspect perceived in the theory of rate-type constitutive models for the specific formulation of the stress tensor in linear and nonlinear thermoelasticity cannot be completely established until the physical meaning of the fractional order and the causality principle are well understood [12,13].

Another important topic in modern engineering is anisotropy. Anisotropic materials comprise most materials in a solid-state body. Beams and plates in a cross-section can be, and in some cases must be, modeled as anisotropic. It is difficult to define the category of anisotropic materials in a convenient manner. However, this term is usually used to describe materials that are neither isotropic nor transversely isotropic. Anisotropy occurs in materials such as single crystals, rolled pentagonal structures, etc. Anisotropic materials have 4 elastic constants, so there are 21 independent elastic constants for general materials. The permissible anisotropic qualities are determined by the symmetry of the coefficients of the elastic component in the formulation of the deformation equilibrium equation [14,15]. If symmetry conditions on each component's elastic coefficients are considered, then the strain energy function can identify numerous types of anisotropy and their associations [16,17].

The concept of generalized thermoelasticity theories was introduced separately in 1972 and 1970. The reasons for generalizing the theory originated from the fact that the mathematical opponent of the simple theory was faced while solving the problem of the relative size of the thermal field and the premise upon which the theory was founded [18,19]. The mechanical portion of the thermodynamic surface of elastic materials, as well as the first full set of thermodynamic balances that offer motion equations, extended Hooke's law, the energy equation, and other results, serves as the foundation for classical thermoelasticity theory [20–22]. The thermal field enters only the second rank of the dissipation functional through entropy and entropy balance, which is determined by the dissipation functional's local extreme. To address the issue, a full thermodynamic functional incorporating the thermal field was constructed. The presence of the thermodynamic principle and the entire thermodynamic functional in characterizing the thermal behavior of a solid has been discussed [23,24].

To address the first problem in the classical thermo-elasticity (CTE) theory proposed by Duhamel [25] and Neumann [26], which predicts two occurrences that contradict empirical facts, Biot [27] proposed the classical coupled thermo-elasticity (CCTE) theory. Most methods for overcoming the classical theory's unwanted prediction are based on the non-Fourier effect. Lord and Shulman [28] proposed an extended thermoelasticity (ETE) theory with a single relaxation time. Green and Lindsay [29] proposed the temperature rate-dependent thermoelasticity (TRDTE) theory, which incorporates temperature rate as a constitutive variable. Green and Naghdi [30,31] made substantial theoretical advances in the field, developing three models for the generalized thermoelasticity of homogeneous

isotropic materials. Chen and Gurtin [32] and Chen et al. [33,34] proposed heat conduction theory based on conductive and thermodynamic temperatures. Quintanilla [35] conducted extensive research on the two-temperature thermoelasticity theory. Youssef [36] introduced the two-temperature generalized thermoelasticity theory, which has been applied to solve several engineering problems [37–40].

The thermoelastic problem has been studied since the fundamental equations that govern it were deduced. Problems involving a heating source and with or without external forces have been the subject of many analyses. It is difficult to identify the analytical solution for such problems; thus, several numerical methods exist for estimating solutions to these problems [41–45]. In recent years, new methods have proven to be useful when used to thermoelasticity problems [46–49]. All these methods are based on solid mathematical principles and can be automated; however, they often require software to achieve the result. Because not all natural phenomena can be characterized by integer-order partial differential equations, some are represented by fractional partial differential equations (FPDEs). Most fractional differential equations do not have explicit analytical solutions; hence, several researchers have devised numerical solution methodologies for time-fractional partial differential equations (TFPDEs). The boundary element method (BEM) is a numerical technique for solving partial differential equations (PDEs) with time-fractional order. This technique combines boundary integral equations with numerical approximation of boundary integrals. These equations can be obtained from the fundamental solutions to PDEs' differential operators. The most significant advantage of the BEM is that the needed discretization of the domain is one less than that of other numerical approaches. It has significant advantages over traditional methods like the finite element method (FEM) and the finite difference method (FDM). One of the key advantages of the BEM is that it is a boundary-only approach, which means that only the issue's boundary must be discretized, resulting in a one-dimensional problem [50–52]. A two-dimensional problem, for example, requires two dimensions of discretization in the FEM or FDM, whereas the BEM just requires one. This is useful for boundary layer problems, which demand tighter grids in locations with large gradients. The BEM has an even greater advantage for problems with infinite or semi-infinite domains, as it is usually necessary to truncate the domain in the FEM or FDM and introduce artificial boundaries with associated treatments such as adding boundary conditions, whereas this is not the case with the BEM because only the boundary is discretized. Domain discretization in the FEM or FDM also requires mesh production, which can frequently be challenging and a time-consuming task [53–55]. This is especially difficult for complex domains or problems whose domain geometry changes over time. With recent computer improvements, numerical approaches based on boundary integral equations have garnered significant attention due to their success in addressing a variety of two-dimensional issues. The boundary element method (BEM) is a popular numerical technique that has applications in a variety of engineering fields, including fluid mechanics, magnetohydrodynamics, and electrodynamics. Recent advances in the BEM have made it possible to apply this method to increasingly complex issues, such as multi-regions [56–58].

Although the boundary element method (BEM) is widely acknowledged for its best-use scenario in tackling high-dimensional issues, one impediment remains to be overcome to make it more accessible and easier to use [59–61]. This impediment is the need for remedies for low-frequency situations in prospective issues; otherwise, numerical instability will be introduced. In recent decades, several initiatives have been made to address this issue, with most of them focused on the concept of transitioning from the original domains to new ones [62–64]. However, those existing translation methods either rely on operator solutions or generate several integral types for a single state variable. As a result, in practice, they continue to make BEM deployment more challenging. As a result, it is important and

meaningful to develop a transformation method that keeps the benefits of simple boundary-type methods while addressing the numerical instability difficulties of low-frequency instances [65–68]. The scaled coordinate transformation (SCT) is purely a mathematical operation that, like the original coordinate transformation, requires only discretization on the structure's surface while remaining analytical in the radial direction, eliminating the need for half-domain discretization and second derivative computations. The scaled coordinate transformation boundary element method (SCTBEM) uses the same integral types and operations on discretized boundary elements as the conventional BEM. However, with the newly devised coordinate transformation, there is no need to be concerned about low-frequency situations in prospective difficulties. Numerical findings demonstrate that the SCTBEM is robust and accurate, even when dealing with very low wave numbers or very huge structures. In addition, the SCTBEM provides a research topic that is not confined to the BEM. Coordinate transformation is a purely mathematical technique that modifies domain integrals in potential problems while leaving boundary integrals untouched. As a result, the SCTBEM can be used for other domain-type methods that use integrals for state variables that are comparable in form [68,69].

Three-block splitting (TBS) is an FFT-based iterative method for solving the three-dimensional time–domain boundary integral equation of the wave equation that is formulated with respect to the boundary magnetic field. In this equation, the time derivative of the boundary magnetic field appears with minus sign, and thus, it has the time-delayed exponential integrator (TDEI) type. The TBS approximately splits this boundary integral equation into three blocks with respect to the wave number components. The convergence of the TBS iteration depends on the value of the time step. For a large time step, the TBS iteration does not converge. To overcome this difficulty, the TBS iteration is applied first with a coarse time step for a few iterations, and then it is applied with the original time step [70].

In the present paper, we investigated the fundamental solutions of fractional order coupled with anisotropic thermoelasticity in the Laplace domain. The fractional boundary element technique was then formulated using a suitable reciprocal connection to solve the considered problem. The boundary was discretized at the collocation nodes. The original problem's boundary integral equations at these collocation points were then solved using the point collocation method. Finally, we presented the results of the suggested BEM model, which better explained our formulation for 3D thermal stress wave propagation in anisotropic materials.

2. Formulation of the Problem

Based on Cattaneo [71] and Vernotte's [72,73] heat conduction equation and definition of the Caputo derivative, Sherief et al. [74] proposed the following fractional heat conduction equation:

$$-k\nabla T = q(x,\tau) + \overline{\tau}\frac{\partial^a q}{\partial \tau^a},\ 0 < a < 1 \tag{1}$$

In Cartesian coordinates, the governing equations for 3D thermal stress wave propagation in anisotropic materials are [28]

$$C_{ijkl}e_{kl} + \rho F_i - \gamma_{ij}T_{,i} = \rho\ddot{u}_i, \gamma_{ij} = C_{ijkl}\alpha_{kl} \tag{2}$$

$$\begin{aligned} &k\bar{T}_{,kk} = \rho C_e\left(\dot{T} + \tau_0\tfrac{\partial^a}{\partial\tau^a}\dot{T}\right) + \gamma_{ij}T_0\left(\dot{e} + \tau_0\tfrac{\partial^a}{\partial\tau^a}\dot{e}\right) \\ &-\rho C_e\left(Q + \tau_0\tfrac{\partial^a}{\partial\tau^a}Q\right), \end{aligned} \tag{3}$$

$$\sigma_{ij} = C_{ijkl}e_{kl} - \gamma_{ij}T, \tag{4}$$

where

$$Q = Q(x,\tau) = \frac{1-R}{x_0} e^{(-\frac{x_a}{x_0})J(\tau)}, J(\tau) = \frac{J_0\tau}{t_1^2} e^{-\frac{\tau}{t_1}}, \mathrm{a} = 1,2,3 \tag{5}$$

$$e_{ij} = \tfrac{1}{2}\left(u_{i,j} + u_{j,i}\right). \tag{6}$$

$$t_i = \sigma_{ij} n_j, \tag{7}$$

Now, we assume the following conditions:

$$\sigma_{ij} n_j = p_{i0}(x,\tau) \text{ on } \mathbb{C}_1, \tag{8}$$

$$u_i = u_{i0}(x,\tau) \text{ on } \mathbb{C}_2, \mathbb{C}_1 \cup \mathbb{C}_2 = \mathbb{C}, \mathbb{C}_1 \cap \mathbb{C}_2 = \phi \tag{9}$$

$$T = T_0(x,\tau) \text{ on } \mathbb{C}_3, \tag{10}$$

$$T_{,n} = T_{n0}(x,\tau) \text{ on } \mathbb{C}_4, \;\; \mathbb{C}_3 \cup \mathbb{C}_4 = \mathbb{C}, \mathbb{C}_3 \cap \mathbb{C}_4 = \phi \tag{11}$$

By applying Equation (4), the traction vector can be represented as follows:

$$t_i(x,\tau) = \left[C_{ijkl} e_{kl} - \gamma_{ij} T\right] n_j(x) \tag{12}$$

3. Boundary Element Implementation

Function $f(\tau)$ has the following Laplace transform:

$$\bar{f}(t) = \int_0^{+\infty} e^{-t\tau} f(\tau) d\tau. \tag{13}$$

Via the application of the Laplace transform to Equations (2)–(4), we obtain

$$C_{ijkl}\bar{\varepsilon}_{kl} + \rho\bar{F}_i - \gamma_{ij}\bar{T}_{,i} = \rho t^2 \bar{u}_i, \tag{14}$$

$$k\bar{T}_{,kk} = \rho C_e t(1+\tau_0 t^\alpha)\left(\bar{T} + \tfrac{\gamma_{ij} T_0}{\rho C_e}\bar{u}_{,kk} - \tfrac{\bar{Q}}{t}\right), \tag{15}$$

$$\bar{\sigma}_{ij} = C_{ijkl}\bar{\varepsilon}_{kl} - \gamma_{ij}\bar{T}. \tag{16}$$

We now present the vectors of displacement and body force as follows:

$$u_i = \phi_{,i} + \epsilon_{ijk}\psi_{k,j}, \tag{17}$$

$$\psi_{i,i} = 0, \tag{18}$$

$$F_i = X_{,i} + \epsilon_{ijk} Y_{k,j}, \tag{19}$$

$$Y_{i,i} = 0. \tag{20}$$

To obtain the fundamental solutions in the Laplace transform domain, we consider the following two cases:

3.1. Case 1: $Q = Q(x,\tau), F_i = 0$

Based on [75], we obtain

$$\left(\nabla^2 - k_1^2\right)\left(\nabla^2 - k_2^2\right)\bar{\phi}' = -m\frac{\rho C_e}{k}(1+\tau_0 t^\alpha) Q(x,\tau), \tag{21}$$

where k_1^2, k_2^2 are the solutions of the following characteristic equation:

$$\begin{aligned} &kv^4 - \left[(\rho C_e + mak)t(1+\tau_0 t^\alpha) + t^{\alpha+1}\tfrac{k}{c_1^2}\right]v^2 \\ &+t^{\alpha+2}\rho C_e \tfrac{(1+\tau_0 t^\alpha)}{c_1^2} = 0. \end{aligned} \tag{22}$$

Equation (21) has the following solution:

$$\bar{\phi}'(x,t) = -m\rho C_e \frac{(1+\tau_0 t^\alpha)}{(\nabla^2 - k_1^2)(\nabla^2 - k_2^2)} Q(x,\tau). \tag{23}$$

which can be written using the Helmholtz equation $\frac{1}{(\nabla^2 - k^2)}\delta(r) = -\frac{1}{4\pi r}e^{-kr}$ as follows:

$$\bar{\phi}'(x,t) = \frac{m\rho C_e}{4\pi k\left(k_1^2 - k_2^2\right)}(1+\tau_0 t^\alpha)\left(e^{-k_1 r} - e^{-k_2 r}\right). \tag{24}$$

Thus, Equations (17) and (24) yield

$$\overline{u}_i'(x,t) = -\frac{\rho C_e}{kr}\frac{m(1+\tau_0 p^\alpha)}{4\pi\left(k_1^2 - k_2^2\right)}\left[e^{-k_1 r}\left(1+\tfrac{k_1}{r}\right) - e^{-k_2 r}\left(1+\tfrac{k_2}{r}\right)\right]r_{,i}\,, \tag{25}$$

and

$$\overline{T}'(x,t) = \frac{\rho C_e}{kr}\frac{m(1+\tau_0 t^\alpha)}{4\pi\left(k_1^2 - k_2^2\right)}\left[e^{-k_1 r}\left(k_1^2 - \tfrac{t^2}{c_1^2}\right) - e^{-k_2 r}\left(k_2^2 - \tfrac{t^2}{c_2^2}\right)\right]. \tag{26}$$

The Laplace transform was successfully applied to the traction vector to yield (see Appendix A)

$$\begin{aligned} \bar{t}_l'(x,t) = \tfrac{\rho C_e\, C_{ijkl}}{kr}\Big\{ &n_k\left[r_{,l}\, r_{,k}\,\left(g_3 + 3\tfrac{g_1}{r}\right)\tfrac{\delta_{lk}}{r}\right] \\ &+n_l\left[r_{,k}\, r_{,k}\left(g_3 + 3\tfrac{g_1}{r}\right) - \tfrac{3}{r}\right]\Big\}. \end{aligned} \tag{27}$$

3.2. Case 2: $Q = 0, \bar{F}_i^{(j)} = \delta_{ij}\delta(x-y)$

By using the Helmholtz equation, we obtain (see Appendix B)

$$\bar{\phi}^{(j)} = \frac{1}{4\pi c_1^2}\frac{r_{,i}}{r^2}\frac{\delta_{ij}}{\left(k_1^2 - k_2^2\right)}\left[\sum_{n=1}^{2}(-1)^{n-1}E(1+k_n r)e^{-k_n r}\right] + \delta_{ij}\frac{r_i}{r^2}\frac{1}{4\pi t^2} \tag{28}$$

$$E = \frac{\left[k_n^2 - \frac{\rho C_e t(1+\tau_0 t^\alpha)}{k}\right]}{k_n^2}, \tag{29}$$

$$\bar{\psi}_l^{(j)} = \epsilon_{ijl}\left(\tfrac{r_{,i}}{4\pi t^2 r^2}\right)\left[\left(1+\tfrac{tr}{c_2}\right)e^{-\frac{tr}{c_2}} - 1\right], \tag{30}$$

$$\bar{u}_l^{(j)} = \tfrac{U_1\delta_{ij}}{r} + \tfrac{U_2 r_{,i}\, r_{,j}}{r}, \tag{31}$$

$$U_1 = \frac{1}{4\pi t^2}\left(\frac{t^2}{c_2^2} + \frac{t}{rc_2} + \frac{1}{r^2}\right)e^{-\frac{tr}{c_2}} + \sum_{n=1}^{2}(-1)^{n-1}\frac{B_n}{r^2}(1+k_n r)e^{-k_n r}, \tag{32}$$

$$U_2 = \left[-\frac{1}{4\pi t^2}\left(\frac{t^2}{c_2^2} + 3\frac{t}{rc_2} + 3\frac{1}{r^2}\right)e^{-\frac{tr}{c_2}}\right] + \sum_{n=1}^{2}(-1)^{n-1}\frac{B_n}{r^2}\left(k_n^2 + 3\frac{k_n}{r} + \frac{3}{r^2}\right)e^{-k_n r}, \tag{33}$$

$$B_n = \tfrac{1}{k_n^2 c_1^2}\tfrac{1}{\left(k_1^2 - k_2^2\right)}\left(k_n^2 - \tfrac{\rho C_e t(1+\tau_0 t^\alpha)}{k}\right). \tag{34}$$

In the absence of a heat source, we find

$$\bar{T}^{(j)} = G\sum_{n=1}^{2}(-1)^{n-1}e^{-k_n r}(1+k_n r)\frac{r_{,i}}{r^2}, \tag{35}$$

where

$$\mathrm{G} = \frac{\delta_{ij}}{4\pi c_1^2}\frac{t(1+\tau_0 t^{\alpha})}{(k_2^2-k_1^2)}.$$

Now, we establish that the temperature in Case 2 is proportional to the displacement in Case 1 as follows:

$$\bar{T}^{(j)} = \frac{\rho t\epsilon}{m\gamma}u_j', \tag{36}$$

where

$$\epsilon = \frac{mak}{\rho C_e}.$$

The traction vector is then obtained in a manner like that used in Case 1

$$\bar{t}_l^{(j)}(x,t) = C_{ijkl}\, n_k\left[\left(\bar{u}_{l,k}^{(j)} + \bar{u}_{k,l}^{(j)}\right) + n_l\left(\bar{u}_{k,k}^{(j)} - \gamma_{ij}\bar{T}^{(j)}\right)\right], \tag{37}$$

where

$$\bar{u}_{i,k}^{(j)} = \frac{U_{1,k}}{r}\delta_{ij} - \frac{U_1\delta_{ij}}{r^2} + \frac{U_{2,k}}{r^2}r_{,i}r_{,j} - \frac{U_2}{r^2}r_{,i}r_{,j}\,r_{,k} + \frac{U_2}{r}r_{,ik}r_{,j} + \frac{U_2}{r}r_{,i}r_{,jk}\,, \tag{38}$$

$$\begin{aligned} U_{1,k} &= \sum_{n=1}^{2}(-1)^{n-1}B_n e^{-k_n r}\frac{r_{,k}}{r}\left[-k_n^2 - 2\frac{(1+k_n r)}{r^2}\right] \\ &+ \frac{r_{,k}}{4\pi t^2}e^{\frac{-tr}{c_2}}\left[-\frac{t^3}{c_2^3} - 2\frac{t}{r^2 c_2} - \frac{2}{r^3} - \frac{t^2}{c_2^2 r}\right], \end{aligned} \tag{39}$$

$$\begin{aligned} U_{2,k} &= -\frac{r_{,k}}{4\pi t^2}e^{\frac{-tr}{c_2}}\left[-\frac{t^3}{c_2^3} - 6\frac{t}{r^2 c_2} - \frac{6}{r^2} - 3\frac{t^2}{c_2^2 r}\right] \\ &+ \sum_{n=1}^{2}(-1)^{n-1}B_n e^{-k_n r}r_{,k}\left[-k_n^2 - 6\frac{k_n}{r^2} - 3\frac{k_n^2}{r} - \frac{6}{r^3}\right]. \end{aligned} \tag{40}$$

Sherief et al. [74] introduced the following reciprocal relation:

$$\begin{aligned} &\tfrac{\rho T_0 p(1+\tau_0 p^{\alpha})}{k}\int_{\mathbb{R}}\left[\bar{F}_i^{(1)}\bar{u}_i^{(2)} - \bar{F}_i^{(2)}\bar{u}_i^{(1)}\right]\mathrm{d}\mathbb{R} \\ &-\tfrac{\rho C_e(1+\tau_0 p^{\alpha})}{k}\int_{\mathbb{R}}\left[\bar{Q}^{(1)}\bar{T}^{(2)} - \bar{Q}^{(2)}\bar{T}^{(1)}\right]\mathrm{d}\mathbb{R} \\ &= \int_{\mathbb{C}_3}\left[\bar{T}^{(1)}\bar{T}_n^{(2)} - \bar{T}^{(2)}\bar{T}_{,n}^{(1)}\right]\mathrm{d}\mathbb{C} \\ &+\int_{\mathbb{C}_4}\left[\bar{T}^{(1)}\bar{T}_n^{(2)} - \bar{T}^{(2)}\bar{T}_n^{(1)}\right]\mathrm{d}\mathbb{C} - \tfrac{T_0 p(1+\tau_0 p^{\alpha})}{k} \\ &\times\left\{\int_{\mathbb{C}_1}\left[\bar{\sigma}_{ij}^{(1)}\bar{u}_i^{(2)} - \bar{\sigma}_{ij}^{(2)}\bar{u}_i^{(1)}\right]n_j\,\mathrm{d}\mathbb{C}\right. \\ &\left.+\int_{\mathbb{C}_2}\left[\bar{\sigma}_{ij}^{(1)}\bar{u}_i^{(2)} - \bar{\sigma}_{ij}^{(2)}\bar{u}_i^{(1)}\right]n_j\,\mathrm{d}\mathbb{C}\right\}. \end{aligned} \tag{41}$$

To describe the displacement and temperature integral equation with respect to the specified functions $\bar{t}_{i0}, \bar{u}_{i0}, \bar{T}_0, \bar{T}_{n0}$, fundamental solutions $\bar{u}_i', \bar{T}'$, $\bar{u}_i^{(j)}$, $\bar{T}(j)$ and their values $\bar{u}_{i0}', \bar{T}_0'$, $\bar{u}_{i0}^{(j)}$, $\bar{T}_0^{(j)}$ on $\mathbb{C}$, we consider Case 1 ($\bar{F}_i = 0$ and $\bar{Q} = \delta(x-y)$) and Case 2 ($\bar{F}_i = \delta_{ij}\delta(x-y)$ and $\bar{Q} = 0$) below.

For case 1, Equation (41) becomes

$$\begin{aligned}&(1+\tau_0 t^a)\Delta(x)\bar{T}(x,t)\\&=\tfrac{k}{\rho C_e}\left\{\int\limits_{\mathbb{C}_3}\left[\bar{T}_0'\bar{T}_n-\bar{T}_0\bar{T}_{n0}'\right]\mathrm{d}\mathbb{C}+\int\limits_{\mathbb{C}_4}\left[\bar{T}'\bar{T}_{n0}-\bar{T}\bar{T}_{,n}'\right]\mathrm{d}\mathbb{C}\right\}-\tfrac{T_0}{\rho C_e}t(1+\tau_0 t^a)\\&\times\left\{\int\limits_{\mathbb{C}_1}\left[t_{i0}\bar{u}_i'-\bar{t}_{i0}'\bar{u}_i\right]\mathrm{d}\mathbb{C}+\int\limits_{\mathbb{C}_2}\left[\bar{\sigma}_{ij}\bar{u}_{i0}'-\bar{\sigma}_{ij}'\bar{u}_{i0}\right]n_j\mathrm{d}\mathbb{C}\right\}\\&-\tfrac{T_0}{C_e}(t+\tau_0 t^\alpha)\int\limits_{\mathbb{R}}\bar{F}_i\bar{u}_i'\mathrm{d}\mathbb{R}+(1+\tau_0 t^a)\int\limits_{\mathbb{R}}\bar{Q}'\bar{T}'\mathrm{d}\mathbb{R}\end{aligned}\tag{42}$$

where

$$\int\limits_{\mathbb{R}}\delta(x-y)\mathrm{d}\mathbb{R}(y)=\Delta(x)=\begin{cases}1, x\in\mathbb{R}\\0,\ x\notin(\mathbb{R}\cup\mathbb{C}),\\\frac{1}{2}, x\in\mathbb{C}\end{cases}$$

For Case II, Equation (41) can be expressed as

$$\begin{aligned}&p(1+\tau_0 p^\alpha)\Delta(x)\bar{u}_j(x,p)=\tfrac{k}{\rho T_0}\left\{\int\limits_{\mathbb{C}_3}\left[\bar{T}_0\bar{T}_{,n}^{(j)}-\bar{T}_0^{(j)}\bar{T}_{,n}\right]\mathrm{d}\mathbb{C}\right.\\&\left.+\int\limits_{\mathbb{C}_4}\left[\bar{T}\bar{T}_{n0}^{(j)}-\bar{T}^{(j)}\bar{T}_{n0}\right]\mathrm{d}\mathbb{C}\right\}+\tfrac{1}{\rho}p(1+\tau_0 p^\alpha)\left\{\int\limits_{\mathbb{C}_1}\left[\bar{p}_{i0}\bar{u}_i^{(j)}-\bar{p}_{i0}^{(j)}\bar{u}_{i0}\right]\mathrm{d}\mathbb{C}\right.\\&\left.+\int\limits_{\mathbb{C}_2}\left[\bar{\sigma}_{il}\bar{u}_{i0}^{(j)}-\bar{\sigma}_{il}^{(j)}\bar{u}_{i0}\right]n_j\mathrm{d}\mathbb{C}\right\}-p(1+\tau_0 p^\alpha)\int\limits_{\mathbb{R}}\bar{F}_i\bar{u}_i^{(j)}\mathrm{d}\mathbb{R}-\tfrac{C_e}{T_0}(1+\tau_0 p^\alpha)\int\limits_{\mathbb{R}}\bar{Q}\bar{T}^{(j)}\mathrm{d}\mathbb{R}\end{aligned}\tag{43}$$

Equation (42) can be solved by using the inverse Laplace transform as follows:

$$L^{-1}(\bar{F}_1(t)\bar{F}_2(t))=\int\limits_0^t F_1(\overline{\tau})F_2(\overline{\tau})d\tau,$$

we arrive at

$$\Delta(x)\left[T(x,\tau)+\tau_0\frac{\partial^a}{\partial\tau^a}T(x,\tau)\right]=M_1(x,\tau),\tag{44}$$

where

$$\begin{aligned}&M_1(x,\tau)=\tfrac{k}{\rho C_e}\int\limits_0^\tau\left\{\int\limits_{\mathbb{C}_3}\left[T_0'(y,\tau-\overline{\tau})T_{,n}(y,x,\overline{\tau})-T_0(y,x,\overline{\tau})T_{,n}'(y,\tau-\overline{\tau})\right]\mathrm{d}\mathbb{C}\right.\\&\left.+\int\limits_{\mathbb{C}_4}\left[T'(y,\tau-\overline{\tau})T_{n0}(y,x,\overline{\tau})-T(y,x,\overline{\tau})T_{n0}'(y,\tau-\overline{\tau})\right]\mathrm{d}\mathbb{C}\right\}d\overline{\tau}\\&+\tfrac{T_0}{\rho C_e}\int\limits_0^\tau\left\{\int\limits_{\mathbb{C}_1}\left[p_{i0}(y,x,\overline{\tau})\left(\tfrac{\partial}{\partial\overline{\tau}}+\tau_0\tfrac{\partial^{a+1}}{\partial\overline{\tau}^{a+1}}\right)u_i'(y,\tau-\overline{\tau})\right]\mathrm{d}\mathbb{C}\right.\\&\left.\times\int\limits_{\mathbb{C}_2}\left[\sigma_{ij}(y,\tau-\overline{\tau})\left(\tfrac{\partial}{\partial\overline{\tau}}+\tau_0\tfrac{\partial^{a+1}}{\partial\overline{\tau}^{a+1}}\right)u_{i0}'(y,x,\overline{\tau})\right]\mathrm{d}\mathbb{C}\right\}d\overline{\tau}\\&-\tfrac{T_0}{\rho C_e}\int\limits_0^\tau\left\{\int\limits_{\mathbb{C}_1}u_i(y,x,\overline{\tau})\left(\tfrac{\partial}{\partial\overline{\tau}}+\tau_0\tfrac{\partial^{a+1}}{\partial\overline{\tau}^{a+1}}\right)p_{i0}'(y,\tau-\overline{\tau})\mathrm{d}\mathbb{C}\right.\\&\left.+\int\limits_{\mathbb{C}_2}u_{i0}(y,\tau-\overline{\tau})\left(\tfrac{\partial}{\partial\overline{\tau}}+\tau_0\tfrac{\partial^{a+1}}{\partial\overline{\tau}^{a+1}}\right)\sigma_{ij}'(y,x,\overline{\tau})\mathrm{d}\mathbb{C}\right\}d\overline{\tau}\\&+\tfrac{T_0}{C_e}\int\limits_0^\tau\int\limits_{\mathbb{R}}F_i(y,\tau-\overline{\tau})\left(\tfrac{\partial}{\partial\overline{\tau}}+\tfrac{\partial^{a+1}}{\partial\overline{\tau}^{a+1}}\right)u_i'(y,x,\overline{\tau})\mathrm{d}\mathbb{R}d\overline{\tau}\\&+\int\limits_0^\tau\int\limits_{\mathbb{R}}Q(y,\tau-\overline{\tau})\left(1+\tfrac{\partial^a}{\partial\overline{\tau}^a}\right)T'(y,x,\overline{\tau})\mathrm{d}\mathbb{R}d\overline{\tau}.\end{aligned}\tag{45}$$

The solution of (44) yields

$$T(x,\tau) = \frac{1}{\Delta x \tau_0}\left[\int_0^{\overline{\tau}} E_{\alpha,\alpha}\left(-\frac{1}{\tau_0}\overline{\tau}^a\right) M_1(x,\tau-\overline{\tau})d\overline{\tau}\right], \tag{46}$$

Where Mittag–Leffler function $E_{\alpha,\alpha}(z)$ is defined as follows [76]:

$$E_{\alpha,\beta}(z) = \sum_{k=0}^{\infty} \frac{z^k}{\Gamma(\alpha k+\beta)}. \tag{47}$$

Similarly, from Equation (43), we obtain

$$\Delta(x)\left[u_j(x,\tau) + \tau_0 \frac{\partial^\alpha}{\partial t^\alpha} u_j(x,\tau)\right] = M_2(x,\tau), \tag{48}$$

where

$$\begin{aligned}
M_2(x,\tau) = {} & \tfrac{k}{\rho T_0}\int_0^{\tau}\left\{\int_{\mathbb{C}_3}\left[T_0(y,x,\overline{\tau})\tfrac{\partial u_j'(y,\tau-\overline{\tau})}{\partial n} - u_j'(y,\tau-\overline{\tau})\tfrac{\partial T(y,x,\overline{\tau})}{\partial n}\right]\mathrm{d}\mathbb{C}\right. \\
& + \int_{\mathbb{C}_4}\left[T(y,x,\overline{\tau})\tfrac{\partial u_j'(y,\tau-\overline{\tau})}{\partial n} - u_j'(y,\tau-\overline{\tau})T_{n0}(y,x,\overline{\tau})\right]\mathrm{d}\mathbb{C}\Big\}d\overline{\tau} \\
& - u_j'(y,\tau-\overline{\tau})T_{n0}(y,x,\overline{\tau})\Big]\mathrm{d}\mathbb{C}\Big\}d\overline{\tau} + \tfrac{1}{\rho}\int_0^{\tau}\left\{\int_{\mathbb{C}_1}\left[p_{i0}(y,x,\overline{\tau})\left(1+\tau_0\tfrac{\partial^a}{\partial\overline{\tau}^a}\right)u_i^{(j)}(y,\tau-\overline{\tau})\mathrm{d}\mathbb{C}\right]\right. \\
& + \int_{\mathbb{C}_2}\left[\sigma_{il}(y,\tau-\overline{\tau})\left(1+\tau_0\tfrac{\partial^a}{\partial\overline{\tau}^a}\right)u_{i0}^{(j)}(y,x,\overline{\tau})n_l\mathrm{d}\mathbb{C}\right]\Big\}d\overline{\tau} \\
& - \tfrac{1}{\rho}\Big\{\int_0^{\tau}\int_{\mathbb{C}_1} u_i(y,x,\overline{\tau})\left(1+\tfrac{\partial^a}{\partial\overline{\tau}^a}\right)p_{i0}^{(j)}(y,\tau-\overline{\tau})\mathrm{d}\mathbb{C} \\
& + \int_{\mathbb{C}_2} u_{i0}(y,\tau-\overline{\tau})\left(1+\tfrac{\partial^a}{\partial\overline{\tau}^a}\right)\sigma_{il}^{(j)}(y,x,\overline{\tau})n_l\mathrm{d}\mathbb{C}\Big\}d\overline{\tau} \\
& + \int_{\mathbb{R}} F_i(y,\tau-\overline{\tau})\left(1+\tau_0\tfrac{\partial^a}{\partial\overline{\tau}^a}\right)u_i^{(j)}(y,x,\tau-\overline{\tau})\mathrm{d}\mathbb{R}d\overline{\tau} \\
& - \int_0^{\tau}\int_{\mathbb{R}} Q(y,\tau-\overline{\tau})\left(1+\tau_0\tfrac{\partial^a}{\partial\overline{\tau}^a}\right)u_j'(y,x,\tau-\overline{\tau})\mathrm{d}\mathbb{R}d\overline{\tau}
\end{aligned} \tag{49}$$

By solving Equation (48), we obtain

$$u_j(x,\tau) = \frac{1}{\Delta x \tau_0}\left[\int_0^{\tau} E_{\alpha,\alpha}\left(-\frac{1}{\tau_0}\overline{\tau}^\alpha\right) M_2(x,\tau-\overline{\tau})d\overline{\tau}\right] \tag{50}$$

Consider the $\lim_{x\to\xi} T(x,\tau)$ of (46) and $\lim_{x\to\xi} u_j(x,\tau)$ of (50). Thus, we have

$$T(\xi,\tau) = \tfrac{2}{\tau_0}\left[\int_0^{\tau} E_{\alpha,\alpha}\left(-\tfrac{1}{\tau_0}\overline{\tau}^\alpha\right) M_1(\xi,\tau-\overline{\tau})d\overline{\tau}\right],\ \xi\in\mathbb{C} \tag{51}$$

$$u_j(\xi,\tau) = \tfrac{2}{\tau_0}\left[\int_0^{\tau} E_{\alpha,\alpha}\left(-\tfrac{1}{\tau_0}\overline{\tau}^\alpha\right) M_2(\xi,\tau-\overline{\tau})d\overline{\tau}\right]\ .\xi\in\mathbb{C} \tag{52}$$

The resulting linear systems were solved using the iteration approach of three-block splitting (TBS) [77].

Figure 1 shows the proposed BEM algorithm flowchart.

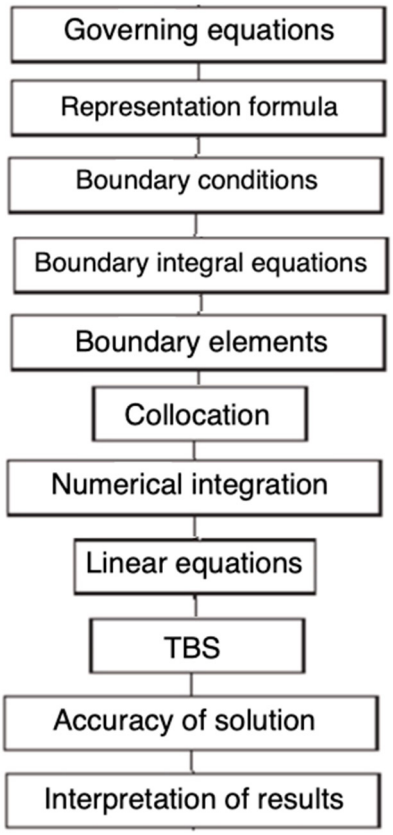


Figure 1. Flowchart of the considered BEM model.

This study focuses on the computational domain, which has 40 boundary nodes and 81 interior nodes, as indicated in Figure 2.

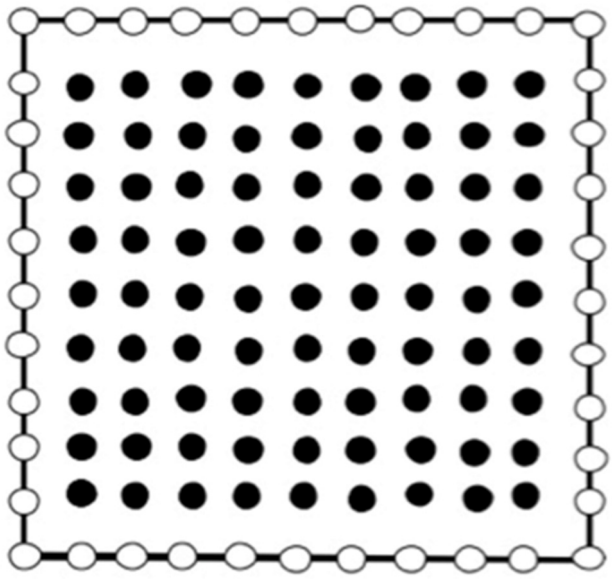


Figure 2. BEM model of the considered problem.

4. Numerical Results and Discussion

To exemplify the numerical findings provided by the proposed methodology, an anisotropic alumina (Al_2O_3) was studied, which had the following properties [14]:

Anisotropic elasticity tensor

$$C = \begin{pmatrix} 576.985 & 75.162 & 132.224 & 47.259 & -37.651 & -1.616 \\ 75.162 & 583373 & 57.046 & -29.680 & -32.710 & 83.907 \\ 132.224 & 57.046 & 519.778 & -12.175 & 85.817 & -54.890 \\ 47.259 & -29.680 & -12.175 & 113.191 & -33.962 & -20.906 \\ -37.651 & -32.710 & 85.817 & -33.962 & 240.907 & 51.386 \\ -1.616 & 83.907 & -54.890 & -20.906 & 51.386 & 188.834 \end{pmatrix} \quad (53)$$

Thermal moduli

$$\begin{aligned} &\gamma_{11} = 2.143(\text{Pa}/^\circ\text{C}), \gamma_{22} = 4.049(\text{Pa}/^\circ\text{C}) \\ &\gamma_{33} = 4.072(\text{Pa}/^\circ\text{C}), \\ &\gamma_{12} = -0.414(\text{Pa}/^\circ\text{C}), \gamma_{13} = -0.024(\text{Pa}/^\circ\text{C}) \end{aligned} \quad (54)$$

Figure 3 shows the distribution of thermal stress σ_{11} wave propagation throughout the x-axis for various fractional parameter values ($a = 0.25$, 0.50, 0.75, and 1.00). The figure shows that the thermal stress σ_{11} waves grow nonlinearly at $0 \leq x \leq 1.5$, then decline linearly and quickly converge to zero at $x = 3$. It is also recognized that when fractional parame a increases, so does σ_{11}. This figure depicts the way the fractional parameter affects the propagation of the thermal stress σ_{12} wave in anisotropic materials.

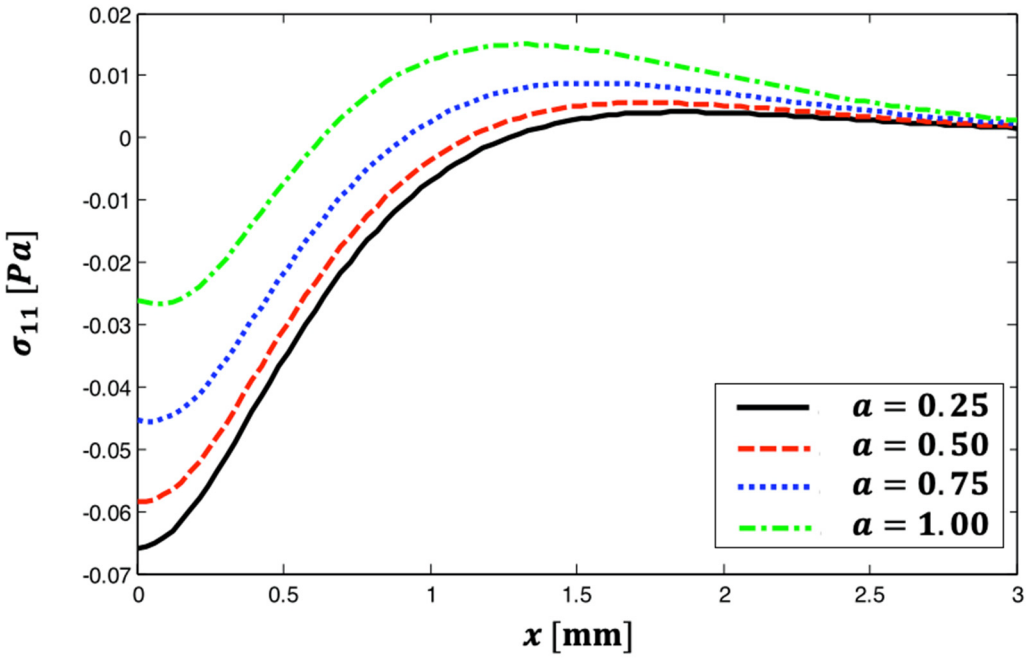


Figure 3. The distribution of thermal stress σ_{11} wave propagation throughout the x-axis for various fractional parameter values.

Figure 4 shows the distribution of thermal stress σ_{12} wave propagation throughout the x-axis for various fractional parameter values ($a = 0.25$, 0.50, 0.75, and 1.00). The image shows that all curves begin at $x = 0$ and rise nonlinearly until they reach a maximum at $0.25 \leq x \leq 0.50$. The function reduces nonlinearly until it reaches a minimal value at $1.0 \leq x \leq 1.5$. The curves then expand linearly until they meet at approximately $x = 3$. It is also noted that σ_{12} diminishes with an increase in fractional parameter a. The figure depicts the way the fractional parameter affects the propagation of the thermal stress σ_{12} wave in anisotropic materials.

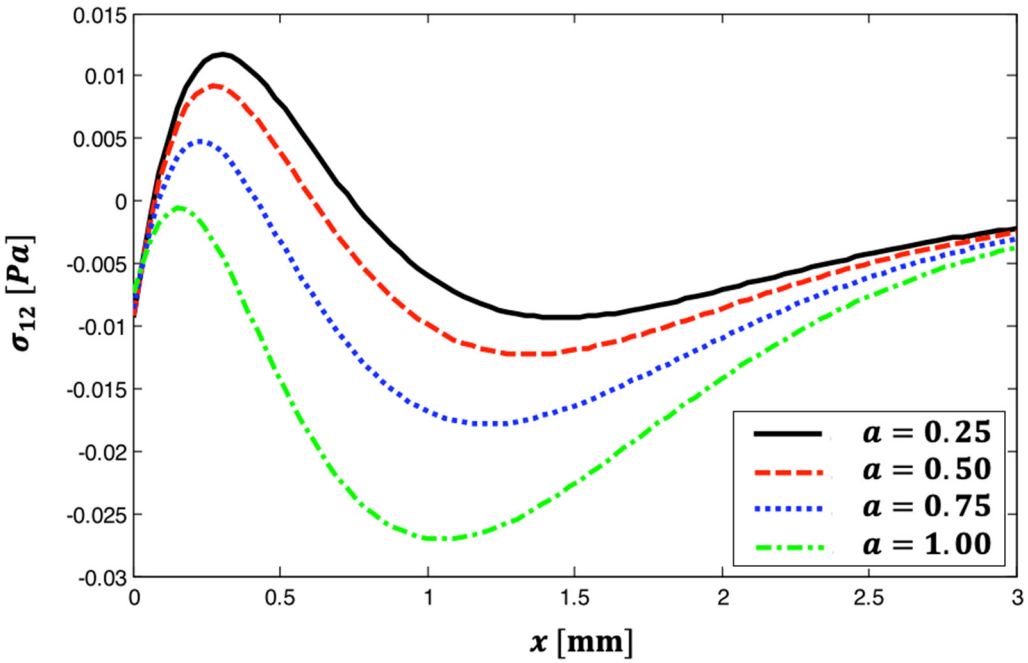


Figure 4. The distribution of thermal stress σ_{12} wave propagation throughout the x-axis for various fractional parameter values.

Figure 5 shows the distribution of thermal stress σ_{22} wave propagation throughout the x-axis for various fractional parameter values ($a = 0.25,\ 0.50,\ 0.75,$ and 1.00). This graphic shows that all curves begin at $x = 0$ and subsequently drop nonlinearly until they reach a minimum at $x = 0.55$. Then, they increase nonlinearly until they meet at around $x = 3$. It is also noted that when the fractional parameter grows, so does σ_{22}. This figure depicts the way the fractional parameter affects the propagation of the thermal stress σ_{22} wave in anisotropic materials.

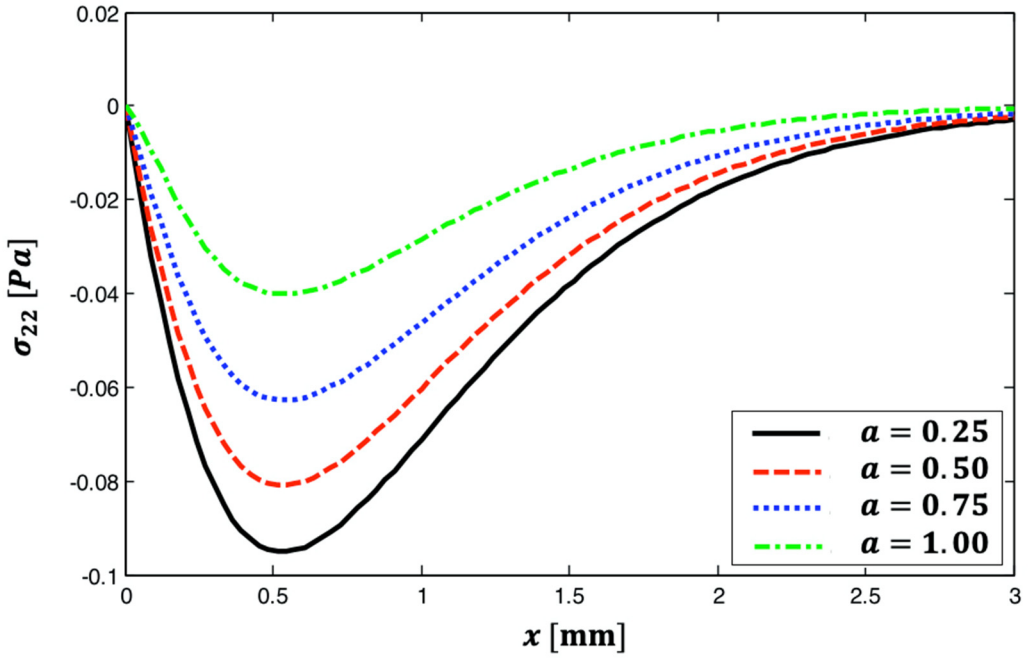


Figure 5. The distribution of thermal stress σ_{22} wave propagation throughout the x-axis for various fractional parameter values.

Figure 6 shows the distribution of thermal stress σ_{13} wave propagation throughout the x-axis for various fractional parameter values ($a = 0.25,\ 0.50,\ 0.75,$ and 1.00). This

graphic shows that all curves begin with a maximum value at $x = 0$, and as the distance increases, these values decrease to practically zero at $x = 3$. Additionally, as the fractional parameter grows, so does σ_{13}. This figure depicts the way the fractional parameter affects the propagation of the thermal stress σ_{13} wave in anisotropic materials.

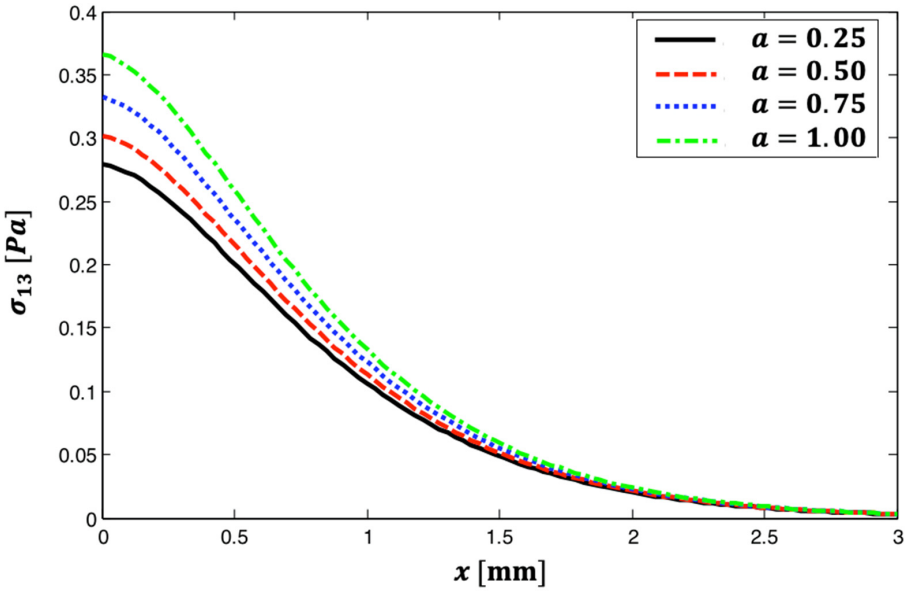


Figure 6. The distribution of thermal stress σ_{13} wave propagation throughout the x-axis for various fractional parameter values.

Figure 7 shows the distribution of thermal stress σ_{23} wave propagation throughout the x-axis for various fractional parameter values ($a = 0.25$, 0.50, 0.75, and 1.00). This image shows that all curves decrease nonlinearly until they reach a minimal value at $0.45 \leq x \leq 0.65$, after which, σ_{23} climbs nonlinearly to approach zero at $x = 3$. Additionally, as the fractional parameter increases, σ_{23} diminishes. The fractional parameter has a substantial impact on thermal stress σ_{23} wave propagation in thermoelastic materials, as illustrated in this figure.

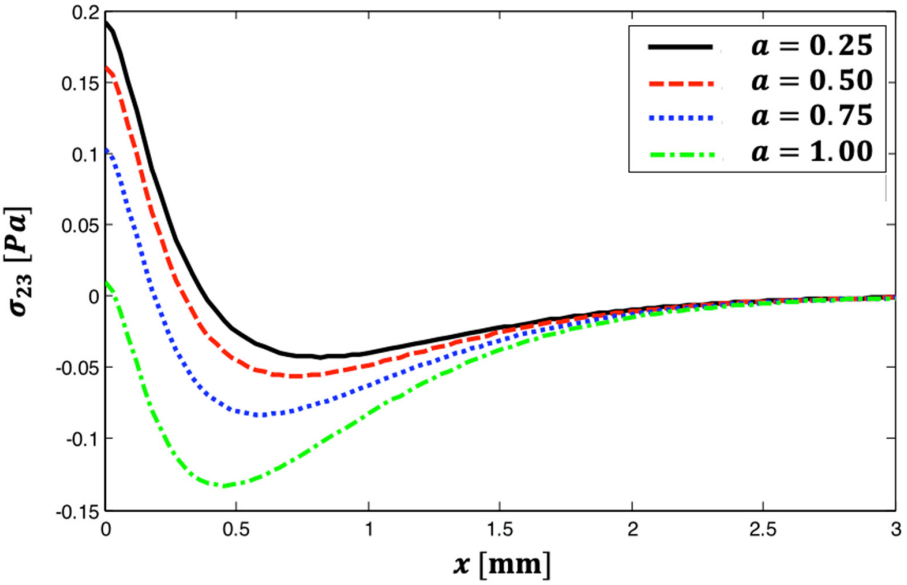


Figure 7. The distribution of thermal stress σ_{23} wave propagation throughout the x-axis for various fractional parameter values.

Figure 8 shows the distribution of thermal stress σ_{33} wave propagation throughout the x-axis for various fractional parameter values ($a = 0.25, 0.50, 0.75,$ and 1.00). This image shows that the curves begin with separate values at $x = 0$, then change and coincide until they reach zero at $x = 3$. It is also noted that when the fractional parameter grows, so does σ_{33}. This graphic illustrates how the fractional parameter affects thermal stress σ_{33} wave propagation in thermoelastic materials.

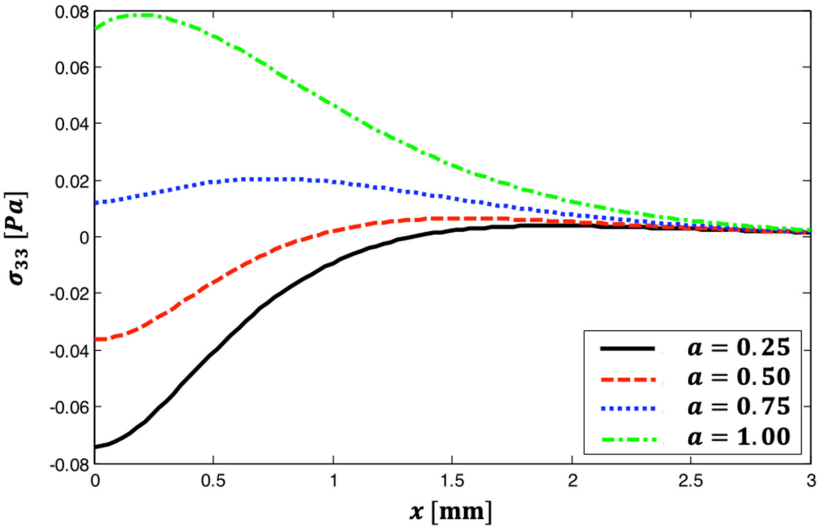


Figure 8. The distribution of thermal stress σ_{33} wave propagation throughout the x-axis for various fractional parameter values.

For validation, we used a particular example of our model and compared our BEM results to Marin et al.'s FEM results [78] and Sharifi's analytical results [79].

Figures 9–11 depict the distributions of thermal stress σ_{11}, σ_{12} and σ_{22} waves propagating throughout the x-axis using BEM, FEM [78] and analytical [79] models. These figures show that the BEM is in excellent agreement with the FEM and analytical methods demonstrating the validity and accuracy of our proposed technique. Matlab R2022a was utilized to generate the computation results for the problem at hand. The proposed fractional boundary element technique in this study is applicable to a wide range of thermal stress wave propagation problems in thermoelastic materials.

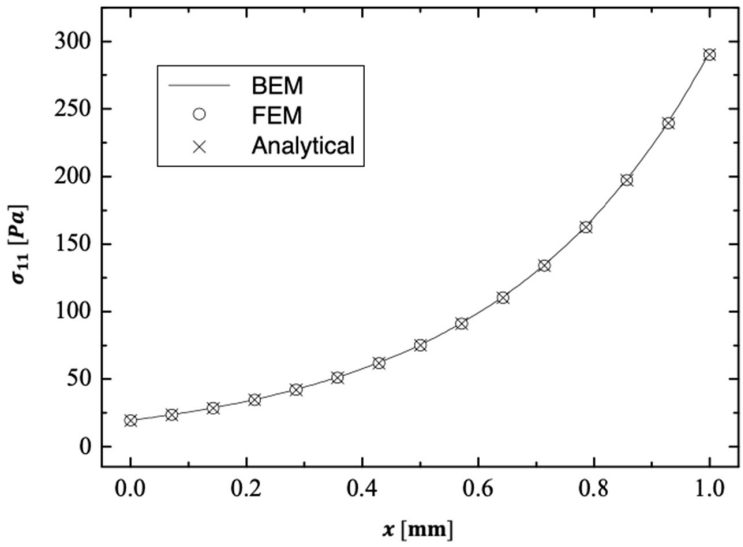


Figure 9. The distribution of thermal stress σ_{11} wave propagation throughout the x-axis using BEM, FEM and analytical methods.

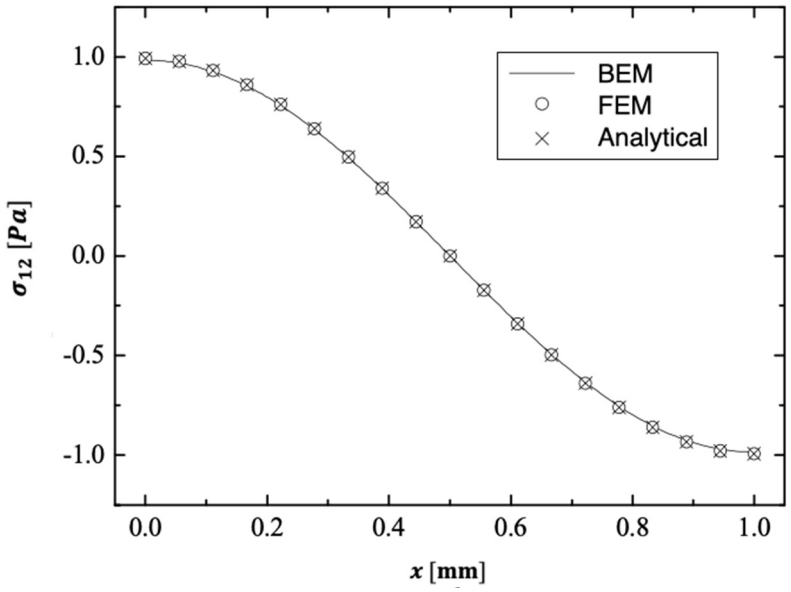


Figure 10. The distribution of thermal stress σ_{12} wave propagation throughout the x-axis using BEM, FEM and analytical methods.

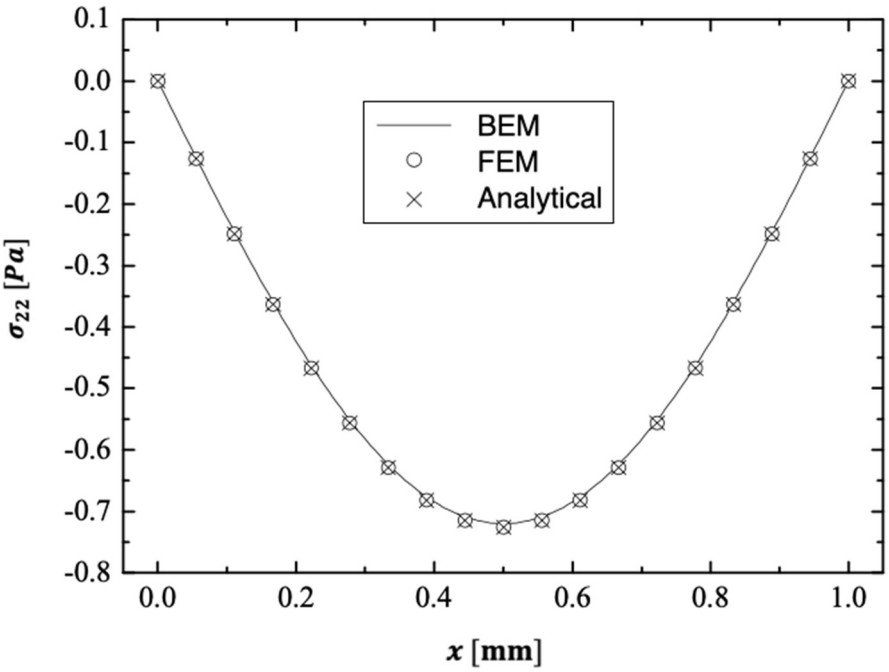


Figure 11. The distribution of thermal stress σ_{22} wave propagation throughout the x-axis using BEM, FEM and analytical methods.

Table 1 displays the CPU time and iteration count for the two-dimensional double successive projection method (2D-DSPM) of Jing and Huang [80], modified symmetric successive overrelaxation (MSSOR) of Darvishi and Hessari [81] and three-block splitting (TBS) of Li et al. [77] iterative methods at each discretization level, with equation numbers in brackets. This table demonstrates that the TBS strategy exceeds both the 2D-DSPM and MSSOR methods.

Table 2 compares the computational requirements for modeling thermal stress wave propagation problems in anisotropic materials using current BEM and FEM approaches [78]. This table demonstrates the efficacy of our proposed BEM approach.

Table 1. CPU timings and iterations for different iterative methods.

Discretization Level	Preconditioning Level	2D-DSPM			MSSOR			TBS		
		CPU Time	Iteration Number	Error	CPU Time	Iteration Number	Error	CPU Time	Iteration Number	Error
1 (36)	0	0.07	8	0.0099	0.08	8	0.0098	0.05	8	0.0098
2 (72)	0	0.19	9	0.0098	0.23	9	0.0097	0.16	8	0.0094
	1	0.16	7	0.0097	0.19	7	0.0096	0.11	7	0.0090
3 (144)	0	0.52	10	0.0095	0.62	11	0.0091	0.42	10	0.0085
	1	0.47	8	0.0092	0.52	9	0.0087	0.34	6	0.0080
	2	0.44	6	0.0088	0.48	7	0.0084	0.30	4	0.0078
4 (288)	0	2.42	13	0.0090	2.52	17	0.0086	1.88	11	0.0084
	1	1.90	11	0.0084	2.10	15	0.0080	1.58	7	0.0078
	2	1.62	7	0.0080	1.82	11	0.0078	1.42	5	0.0076
	3	1.42	5	0.0078	1.52	7	0.0076	1.38	3	0.0074
5 (576)	0	9.98	15	0.0088	12.04	19	0.0084	7.84	13	0.0082
	1	9.12	11	0.0084	10.12	17	0.0082	6.82	9	0.0080
	2	8.20	9	0.0082	9.32	15	0.0076	6.12	7	0.0075
	3	7.26	7	0.0080	8.48	11	0.0074	5.84	5	0.0073
	4	6.46	5	0.0078	7.01	7	0.0072	5.20	3	0.0070
6 (1152)	0	40.4	19	0.0086	46.6	21	0.0082	34.4	15	0.0080
	1	36.3	17	0.0084	43.0	19	0.0080	32.6	11	0.0078
	2	33.9	15	0.0082	41.0	17	0.0078	30.8	9	0.0076
	3	29.0	11	0.0080	34.9	13	0.0076	29.0	7	0.0074
	4	26.8	9	0.0076	32.8	11	0.0074	22.9	5	0.0072
	5	24.9	7	0.0074	29.0	9	0.0072	21.1	3	0.0070

Table 2. Study of computational power requirements for modeling thermal stress wave propagation problems in anisotropic materials utilizing current BEM and FEM.

	BEM	FEM
Number of nodes	54	56,000
Number of elements	18	9000
CPU time [min]	2	200
Memory [Mbyte]	1	140
Disk space [Mbyte]	0	260
Accuracy of results [%]	1.0	2.3

5. Conclusions

The primary goal of this paper was to present a novel fractional boundary element method (BEM) formulation for solving thermal stress wave propagation problems in anisotropic materials. In the Laplace domain, the fundamental solutions to the governing equations could be found. The boundary integral equations were then built. The heat conduction equation under consideration was formulated using the Caputo fractional time derivative. The resulting BEM linear systems were solved using the three-block splitting (TBS) iteration strategy, which required fewer iterations and consumed less CPU time. The new TBS iteration approach converged quickly and did not require complex computations. It outperformed the two-dimensional double successive projection method (2D-DSPM) and modified symmetric successive overrelaxation (MSSOR) in solving the resultant BEM linear system. We only looked at one specific scenario of our model to compare our results to those of other publications in the literature. Because the BEM results were so compatible with the finite element method (FEM) and analytical findings, the numerical results showed that our proposed BEM formulation was valid, accurate, and efficient in handling three-dimensional thermal stress wave propagation problems in anisotropic materials. The current research has several applications, including nuclear physical science, biophysics, geothermal engineering, pressure vessels, econophysics, biochemistry, robotics and control theory, food engineering, signal and image processing, aviation, electronics, and many more.

Author Contributions: Conceptualization, M.A.F.; Methodology, M.A.F.; Software, M.A.F.; Validation, M.A.F.; Formal analysis, M.A.F.; Investigation, M.A.F.; Resources, M.A.F. and M.T.; Data curation, M.A.F.; Writing—original draft, M.A.F. and M.T.; Writing—review & editing, M.A.F. and M.T. All authors have read and agreed to the published version of the manuscript.

Funding: This research received no external funding.

Data Availability Statement: All data generated or analyzed during this study are included in this published article.

Conflicts of Interest: The authors declare no conflicts of interest.

Nomenclature

α_{kl}	Coefficients of thermal expansion
γ_{ij}	$= C_{ijkl}\alpha_{kl}$ thermal moduli
δ_{ij}	Kronecker delta
e_{ij}	Strains
σ_{ij}	Stress
τ	Time
a	Fractional-order parameter
C_{ijkl}	Elastic constants
C_e	Specific heat at constant strain
$\mathbb{C}$	$= \mathbb{C}_1 \cup \mathbb{C}_2 = \mathbb{C}_3 \cup \mathbb{C}_4$ boundary
e	$= e_{kk}$ dilatation
F_i	Body force vector
$J(\tau)$	Non-Gaussian temporal profile
J_0	Total energy intensity
k	Thermal conductivity
n_j	Outward normal components
$Q(x,\tau)$	Heat source intensity
R	Irradiated surface absorptivity
r	$= \sqrt{(x_i - y_i)(x_i - y_i)}$ radial distance
$r_{,i}$	$= \frac{(x_i - y_i)}{r}$
T	Temperature
$\bar{T}^{(j)}$	Temperature fundamental solutions
T_0	Reference temperature
t_1	Laser pulse time characteristic
u_j	Displacement vector
$\bar{u}_i^{(j)}$	Displacement fundamental solutions
x	$= (x_1, x_2, x_3)$

Appendix A. Laplace Transform Implementation

The traction vector on $\mathbb{C}$ can be expressed as

$$t_i(x,\tau) = \left[C_{ijkl}e_{kl} - \gamma_{ij}T\right]n_j(x) \tag{A1}$$

The Laplace transform was successfully applied to the traction vector (A1) to yield

$$\bar{t}_i(x,\tau) = \left[C_{ijkl}\bar{e}_{kl} - \gamma_{ij}\bar{T}\right]n_i(x). \tag{A2}$$

$$\overline{u}_i'(x,t) = -\frac{\rho C_e}{kr}\frac{m(1+\tau_0 p^\alpha)}{4\pi(k_1^2 - k_2^2)}\left[e^{-k_1 r}\left(1 + \frac{k_1}{r}\right) - e^{-k_2 r}\left(1 + \frac{k_2}{r}\right)\right]r_{,i}, \tag{A3}$$

The derivative of Equation (A3) gives

$$\bar{u}'_{i,j} = -\frac{\rho C_e}{k}\left[\frac{r_{,i}}{r}g_{1,j} - \frac{\left(r_{,j}\, r_{,i}\, g_1 - r\, r_{,ij} g_1\right)}{r^2}\right], \tag{A4}$$

where

$$g_1 = \frac{m(1+\tau_0 t^\alpha)}{4\pi\left(k_1^2-k_2^2\right)}\left[e^{-k_1 r}\left(1+\frac{k_1}{r}\right) - e^{-k_2 r}\left(1+\frac{k_2}{r}\right)\right], \tag{A5}$$

and

$$\begin{aligned} g_{1,j} = \frac{m(1+\tau_0 t^\alpha)}{4\pi\left(k_1^2-k_2^2\right)}\Big[&-k_1 e^{-k_1 r} r_{,j}\left(1+\tfrac{1}{r^2}\right) \\ &-k_1^2 e^{-k_1 r}\tfrac{r_{,j}}{r} + k_2 e^{-k_2 r} r_{,j}\left(1+\tfrac{1}{r^2}\right) - k_2^2 e^{-k_2 r}\tfrac{r_{,j}}{r}\Big]. \end{aligned} \tag{A6}$$

Equation (A4) may be expressed as

$$\bar{u}'_{i,j} = \frac{m(1+\tau_0 t^\alpha)}{4\pi\left(k_1^2-k_2^2\right)}\left[r_{,i} r_{,j}\frac{g_3}{r} - \frac{1}{r^2}\left(\delta_{ij} - 3 r_{,i}\, r_{,j}\right) g_1\right], \tag{A7}$$

where

$$g_3 = \frac{(1+\tau_0 t^\alpha)}{4\pi\left(k_1^2-k_2^2\right)}\left[k_1^2 e^{-k_1 r} - k_2^2 e^{-k_2 r}\right], \tag{A8}$$

Thus, using Equations (A2) and (A7), we obtain

$$\begin{aligned} \bar{t}'_l(x,t) = \frac{\rho C_e\, C_{ijkl}}{kr}\Big\{&n_k\left[r_{,l}\, r_{,k}\left(g_3 + 3\tfrac{g_1}{r}\right)\tfrac{\delta_{lk}}{r}\right] \\ &+ n_l\left[r_{,k}\, r_{,k}\left(g_3 + 3\tfrac{g_1}{r}\right) - \tfrac{3}{r}\right]\Big\}. \end{aligned} \tag{A9}$$

Appendix B. Helmholtz Theorem Implementation

The Helmholtz theorem is applied to vectors $u_i^{(j)}$ and $F_i^{(j)}$ to obtain

$$\bar{u}_i^{(j)} = \bar{\phi}_{,i}^{(j)} + \epsilon_{ilk}\bar{\psi}_{l,k}^{(j)}, \tag{A10}$$

$$\bar{F}_i^{(j)} = \bar{P}_{,i}^{(j)} + \epsilon_{ilk}\bar{R}_{l,k}^{(j)}. \tag{A11}$$

where the potentials $\bar{\phi}^{(j)}$, $\bar{P}^{(j)}$, $\bar{\psi}_l^{(j)}$, and $\bar{R}_i^{(j)}$ satisfy the following relations:

$$\left(\nabla^2 - k_1^2\right)\left(\nabla^2 - k_2^2\right)\bar{\phi}^{(j)} = -\frac{1}{c_1^2}\left[\nabla^2 - \frac{\rho C_e}{k} t\left(1+\tau_0 t^\alpha\right)\right]\bar{P}^{(j)}, \tag{A12}$$

$$\bar{\theta}^{(j)} = \frac{1}{m}\left[\left(\nabla^2 - \frac{t^2}{c_1^2}\right)\bar{\phi}^{(j)} + \frac{\bar{P}^{(j)}}{c_1^2}\right], \tag{A13}$$

$$\left(\nabla^2 - \frac{t^2}{c_1^2}\right)\bar{\psi}_l^{(j)} = -\frac{1}{c_2^2}\bar{R}_i^{(j)}, \tag{A14}$$

The Helmholtz decomposition theorem is used to determine

$$\bar{P}^{(j)} = -\frac{1}{4\pi}\left(\frac{\delta_{ij}}{r}\right)_{,i}, \tag{A15}$$

$$\bar{R}_l^{(j)} = \frac{1}{4\pi}\epsilon_{ilk}\left(\frac{\delta_{ij}}{r}\right)_{,k}. \tag{A16}$$

References

1. Ezzat, M.; Zakaria, M.; Shaker, O.; Barakat, F. State space formulation to viscoelastic fluid flow of magnetohydrodynamic free convection through a porous medium. *Acta Mech.* **1996**, *119*, 147–164. [CrossRef]
2. Ezzat, M.A. Free convection effects on perfectly conducting fluid. *Int. J. Eng. Sci.* **2001**, *39*, 799–819. [CrossRef]
3. Fahmy, M.A. Thermoelastic stresses in a rotating non-homogeneous aniso-tropic body. *Numer. Heat Transf. Part A* **2008**, *53*, 1001–1011. [CrossRef]
4. Abouelregal, A.E.; Mohammed, W.W. Effects of nonlocal thermoelasticity on nanoscale beams based on couple stress theory. *Math. Methods Appl. Sci.* **2020**. [CrossRef]
5. Othman, M.I.A.; Abd-Elaziz, E.M. Dual-phase-lag model on micropolar thermoelastic rotating medium under the effect of thermal load due to laser pulse. *Indian J. Phys.* **2020**, *94*, 999–1008. [CrossRef]
6. Othman, M.I.A.; Zidan, M.E.M.; Mohamed, I.E.A. Dual-phase-lag model on thermo-microstretch elastic solid under the effect of initial stress and temperature-dependent. *Steel Compos. Struct.* **2021**, *38*, 355–363.
7. Bagley, R.L.; Torvik, P.J. On the fractional calculus model of viscoelastic behavior. *J. Rheol.* **1986**, *30*, 133–155. [CrossRef]
8. Machado, J.A.T. Analysis and design of fractional-order digital control systems. *SAMS J. Syst. Anal. Model. Simul.* **1997**, *27*, 107–122.
9. Oldham, K.B.; Spanier, J. *The Fractional Calculus: Theory and Applications of Differentiation and Integration to Arbitrary Order*, 1st ed.; Dover Publication: Mineola, NY, USA, 2006; Volume 111, pp. 1–64.
10. Kilbas, A.A.; Srivastava, H.M.; Trujillo, J.J. *Theory and Applications of Fractional Differential Equations*, 1st ed.; Elsevier Science: Amsterdam, The Netherlands, 2006; Volume 204, pp. 449–463.
11. Sabatier, J.; Agrawal, O.P.; Machado, J.A.T. *Advances in Fractional Calculus: Theoretical Developments and Applications in Physics and Engineering*, 1st ed.; Springer: Dordrecht, The Netherlands, 2007; Volume 1, pp. 169–302.
12. Wang, J.L.; Li, H.F. Surpassing the fractional derivative: Concept of the memory-dependent derivative. *Comput. Math. Appl.* **2011**, *62*, 1562–1567. [CrossRef]
13. Yu, Y.J.; Zhao, L.J. Fractional thermoelasticity revisited with new definitions of fractional derivative. *Eur. J. Mech.—A/Solids* **2020**, *84*, 104043. [CrossRef]
14. Shiah, Y.C.; Tuan, N.A.; Hematiyan, M.R. Direct transformation of the volume integral in the boundary integral equation for treating three-dimensional steady-state anisotropic thermoelasticity involving volume heat source. *Int. J. Solids Struct.* **2018**, *143*, 287–297. [CrossRef]
15. Fahmy, M.A. Boundary element algorithm for nonlinear modeling and simulation of three temperature anisotropic generalized micropolar piezothermoelasticity with memory-dependent derivative. *Int. J. Appl. Mech.* **2020**, *12*, 2050027. [CrossRef]
16. Fahmy, M.A. Boundary element modeling of fractional nonlinear generalized photothermal stress wave propagation problems in FG anisotropic smart semiconductors. *Eng. Anal. Bound. Elem.* **2022**, *134*, 665–679. [CrossRef]
17. Fahmy, M.A.; Shaw, S.; Mondal, S.; Abouelregal, A.E.; Lotfy, K.; Kudinov, I.A.; Soliman, A.H. Boundary Element Modeling for Simulation and Optimization of Three-Temperature Anisotropic Micropolar Magneto-thermoviscoelastic Problems in Porous Smart Structures Using NURBS and Genetic Algorithm. *Int. J. Thermophys.* **2021**, *42*, 29. [CrossRef]
18. Othman, M.I.A.; Atwa, S.Y.; Farouk, R.M. Generalized magneto-thermoviscoelastic plane waves under the effect of rotation without energy dissipation. *Int. J. Eng. Sci.* **2008**, *46*, 639–653. [CrossRef]
19. Othman, M.I.A.; Song, Y. Effect of rotation on plane waves of generalized electro magneto-thermoviscoelasticity with two relaxation times. *Appl. Math. Model.* **2008**, *32*, 811–825. [CrossRef]
20. Ezzat, M.A.; Awad, E.S. Micropolar generalized magneto-thermoelasticity with modified Ohm's and Fourier's laws. *J. Math. Anal. Appl.* **2009**, *353*, 99–113. [CrossRef]
21. Ezzat, M.A.; Youssef, H.M. Generalized magneto-thermoelasticity in a perfectly conducting medium. *Int. J. Solids Struct.* **2005**, *42*, 6319–6334. [CrossRef]
22. Othman, M.I.A.; Eraki, E.E.M. Effect of gravity on generalized thermoelastic diffusion due to laser pulse using dual-phase-lag model. *Multidiscip. Model. Mater. Struct.* **2018**, *14*, 457–481. [CrossRef]
23. Fahmy, M.A. A Nonlinear Fractional BEM Model for Magneto-Thermo-Visco-Elastic Ultrasound Waves in Temperature-Dependent FGA Rotating Granular Plates. *Fractal Fract.* **2023**, *7*, 214. [CrossRef]
24. Fahmy, M.A. A New Boundary Element Strategy for Modeling and Simulation of Three Temperatures Nonlinear Generalized Micropolar-Magneto-Thermoelastic Wave Propagation Problems in FGA Structures. *Eng. Anal. Bound. Elem.* **2019**, *108*, 192–200. [CrossRef]
25. Duhamel, J. Some memoire sur les phenomenes thermo-mechanique. *J. L'école Polytech.* **1837**, *15*, 1–57.
26. Neumann, F. *Vorlesungen Uber die Theorie der Elasticitat*; Meyer: Brestau, Germany, 1885.
27. Biot, M. Thermoelasticity and irreversible thermo-dynamics. *J. Appl. Phys.* **1956**, *27*, 249–253. [CrossRef]
28. Lord, H.W.; Shulman, Y. A generalized dynamical theory of thermoelasticity. *J. Mech. Phys. Solids* **1967**, *15*, 299–309. [CrossRef]
29. Green, A.E.; Lindsay, K.A. Thermoelasticity. *J. Elast.* **1972**, *2*, 1–7. [CrossRef]

30. Green, A.E.; Naghdi, P.M. On undamped heat waves in an elastic solid. *J. Therm. Stress.* **1992**, *15*, 253–264. [CrossRef]
31. Green, A.E.; Naghdi, P.M. Thermoelasticity without energy dissipation. *J. Elast.* **1993**, *31*, 189–208. [CrossRef]
32. Chen, P.J.; Gurtin, M.E. On a theory of heat conduction involving two temperatures. *Z. Angew. Math. Phys. ZAMP* **1968**, *19*, 614–627. [CrossRef]
33. Chen, P.J.; Gurtin, M.E.; Williams, W.O. A note on non-simple heat conduction. *Z. Angew. Math. Phys. ZAMP* **1968**, *19*, 969–970. [CrossRef]
34. Chen, P.J.; Gurtin, M.E.; Williams, W.O. On the thermodynamics of non-simple elastic materials with two temperatures. *Z. Angew. Math. Phys. ZAMP* **1969**, *20*, 107–112. [CrossRef]
35. Quintanilla, R. On existence, structural stability, convergence and spatial behavior in thermoelasticity with two-temperatures. *Acta Mech.* **2004**, *168*, 61–73. [CrossRef]
36. Youssef, H.M. Theory of two-temperature generalized thermoelasticity. *IMA J. Appl. Math.* **2006**, *71*, 383–390. [CrossRef]
37. Youssef, H.M.; Al-Lehaibi, E.A. State-space approach of two-temperature generalized thermoelasticity of one dimensional problem. *Int. J. Solids Struct.* **2007**, *44*, 1550–1562. [CrossRef]
38. Bassiouny, E.; Youssef, H.M. Two-temperature generalized thermopiezoelasticity of finite rod subjected to different types of thermal loading. *J. Therm. Stress.* **2008**, *31*, 233–245. [CrossRef]
39. Youssef, H.M. Two-dimensional problem of two-temperature generalized thermoelastic half-space subjected to ramp-type heating. *Comput. Math. Model.* **2008**, *19*, 201–216. [CrossRef]
40. Fahmy, M.A. Shape design sensitivity and optimization for two-temperature generalized magneto-thermoelastic problems using time-domain DRBEM. *J. Therm. Stress.* **2018**, *41*, 119–138. [CrossRef]
41. Rizzo, F.J.; Shippy, D.J. An advanced boundary integral equation method for three-dimensional thermoelasticity. *Int. J. Numer. Methods Eng.* **1977**, *11*, 1753–1768. [CrossRef]
42. Brebbia, C.A. *The Boundary Element Method for Engineers*; Pentech Press: London, UK, 1978.
43. Brebbia, C.A.; Walker, S. *Boundary Element Method Techniques in Engineering*; Newness-Butterworths: London, UK, 1980.
44. Banerjee, P.K.; Butterfield, R. *Boundary Element Methods in Engineering Science*; McGraw-Hill: London, UK, 1981.
45. Fenner, R.T. Boundary element for stress problems. In *Seminar on Finite Elements or Boundary Elements*; Institution of Mechanical Engineers: London, UK, 1982.
46. Brebbia, C.A.; Tells, J.C.F.; Wrobel, L.C. *Boundary Element Techniques: Theory and Applications in Engineering*; Springer: Heidelberg, Germany, 1984.
47. Sladek, V.; Sladek, J. Boundary integral equation method in two-dimensional thermoelasticity. *Eng. Anal.* **1984**, *1*, 135–148. [CrossRef]
48. Sladek, V.; Sladek, J. Boundary integral equation method in thermoelasticity Part III: Uncoupled thermoelasticity. *Appl. Math. Model.* **1984**, *8*, 413–418. [CrossRef]
49. Cruse, T.A.; Rizzo, F.J. Boundary integral equation methods-computational applications. In *Applied Mechanics, Proceedings of the ASME Conference on Boundary Integral Equation Methods*; ASME: New York, NY, USA, 1985; pp. 118–123.
50. Cao, G.; Yu, B.; Chen, L.; Yao, W. Isogeometric dual reciprocity BEM for solving non-Fourier transient heat transfer problems in FGMs with uncertainty analysis. *Int. J. Heat Mass Transf.* **2022**, *203*, 123783. [CrossRef]
51. Sladek, J.; Sladek, V.; Markechova, I. Boundary element method analysis of stationary thermoelasticity problems in non-homogeneous media. *Int. J. Numer. Methods Eng.* **1990**, *30*, 505–516. [CrossRef]
52. Zhang, S.; Yu, B.; Chen, L. Non-iterative reconstruction of time-domain sound pressure and rapid prediction of large-scale sound field based on IG-DRBEM and POD-RBF. *J. Sound Vib.* **2024**, *573*, 118226. [CrossRef]
53. Tanaka, M.; Matsumoto, T.; Moradi, M. Application of boundary element method to 3-D problems of coupled thermoelasticity. *Eng. Anal. Boundary. Elem.* **1995**, *16*, 297–303. [CrossRef]
54. Ang, W.T.; Clements, D.L.; Cooke, T. A Complex Variable Boundary Element Method for a Class of Boundary Value Problems in Anisotropic Thermoelasticity. *Int. J. Comput. Math.* **1999**, *70*, 571–586. [CrossRef]
55. Shiah, Y.C.; Tan, C.L. Exact boundary integral transformation of the thermoelastic domain integral in BEM for general 2D anisotropic elasticity. *Comput. Mech.* **1999**, *23*, 87–96. [CrossRef]
56. Kogl, M.; Gaul, L. A boundary element method for anisotropic coupled thermoelasticity. *Arch. Appl. Math.* **2003**, *73*, 377–398.
57. El-Naggar, A.M.; Abd-Alla, A.M.; Fahmy, M.A. The propagation of thermal stresses in an infinite elastic slab. *Appl. Math. Comput.* **2004**, *157*, 307–312. [CrossRef]
58. Fahmy, M.A.; Jeli, R.A.A. A New Fractional Boundary Element Model for Anomalous Thermal Stress Effects on Cement-Based Materials. *Fractal Fract.* **2024**, *8*, 753. [CrossRef]
59. Abd-Alla, A.M.; Fahmy, M.A.; El-Shahat, T.M. Magneto-thermo-elastic problem of a rotating non-homogeneous anisotropic solid cylinder. *Arch. Appl. Mech.* **2008**, *78*, 135–148. [CrossRef]
60. Fahmy, M.A. A time-stepping DRBEM for nonlinear fractional sub-diffusion bio-heat ultrasonic wave propagation problems during electromagnetic radiation. *J. Umm Al-Qura Univ. Appl. Sci.* **2024**. [CrossRef]

61. Fahmy, M.A.; Almehmadi, M.M. Fractional Dual-Phase-Lag Model for Nonlinear Viscoelastic Soft Tissues. *Fractal Fract.* **2023**, *7*, 66. [CrossRef]
62. Zhang, S.; Yu, B.; Chen, L.; Lian, H.; Bordas, S.P.A. Isogeometric dual reciprocity BEM for solving time-domain acoustic wave problems; Non-iterative reconstruction of time-domain sound pressure and rapid prediction of large-scale sound field based on IG-DRBEM and POD-RBF. *Comput. Math. Appl.* **2024**, *160*, 125–141. [CrossRef]
63. Fahmy, M.A.; Alzubaidi, M.H.M. A boundary element analysis of quasi-potential inviscid incompressible flow in multiply connected airfoil wing. *J. Umm Al-Qura Univ. Eng. Archit.* **2024**, *15*, 398–402. [CrossRef]
64. Fahmy, M.A.; Toujani, M. Fractional Boundary Element Solution for Nonlinear Nonlocal Thermoelastic Problems of Anisotropic Fibrous Polymer Nanomaterials. *Computation* **2024**, *12*, 117. [CrossRef]
65. Fahmy, M.A.; Alsulami, M.O.; Abouelregalm, A.E. Three-Temperature Boundary Element Modeling of Ultrasound Wave Propagation in Anisotropic Viscoelastic Porous Media. *Axioms* **2023**, *12*, 473. [CrossRef]
66. Fahmy, M.A. Fractional Temperature-Dependent BEM for Laser Ultrasonic Thermoelastic Propagation Problems of Smart Nanomaterials. *Fractal Fract.* **2023**, *7*, 536. [CrossRef]
67. Fahmy, M.A. BEM Modeling for Stress Sensitivity of Nonlocal Thermo-Elasto-Plastic Damage Problems. *Computation* **2024**, *12*, 87. [CrossRef]
68. Yu, B.; Jing, R. SCTBEM: A scaled coordinate transformation boundary element method with 99-line MATLAB code for solving Poisson's equation. *Comput. Phys. Commun.* **2024**, *300*, 109185. [CrossRef]
69. Jing, R.; Yu, B.; Ren, S.; Yao, W. A novel SCTBEM with inversion-free Padé series expansion for 3D transient heat transfer analysis in FGMs. *Comput. Methods Appl. Mech. Eng.* **2025**, *433*, 117546. [CrossRef]
70. Takahashi, T.; Tanigawa, M.; Miyazawa, N. An enhancement of the fast time-domain boundary element method for the three-dimensional wave equation. *Comput. Phys. Commun.* **2022**, *271*, 108229. [CrossRef]
71. Cattaneo, C. A form of heat conduction equation which eliminates the paradox of instantaneous propagation. *Comptes Rendus* **1958**, *247*, 431–433.
72. Vernotte, P. Les paradoxes de la theorie continue de l'equation de la chaleur. *Comptes Rendus* **1958**, *246*, 3154–3155.
73. Vernotte, P. Some possible complications in the phenomena of thermal conduction. *Comptes Rendus* **1961**, *252*, 2190–2191.
74. Sherief, H.H.; El Sayed, A.; El-Latief, A. Fractional Order Theory of Thermoelasticity. *Int. J. Solids Struct.* **2010**, *47*, 269–275. [CrossRef]
75. Tiwari, R.; Mukhopadhyay, S. Boundary integral equations formulation for fractional order thermoelasticity. *Comput. Methods Sci. Eng. CMST* **2014**, *20*, 49–58. [CrossRef]
76. Podlubny, I. *Fractional Differential Equations. An Introduction to Fractional Order Derivatives, Fractional Differential Equations, to Methods of Their Solutions and Some of Their Applications*; Academic Press: Cambridge, MA, USA, 1999; Volume 198.
77. Li, Y.R.; Shao, X.F.; Li, S.Y. New Preconditioned Iteration Method Solving the Special Linear System from the PDE-Constrained Optimal Control Problem. *Mathematics* **2021**, *9*, 510. [CrossRef]
78. Marin, M.; Hobiny, A.; Abbas, I. The Effects of Fractional Time Derivatives in Porothermoelastic Materials Using Finite Element Method. *Mathematics* **2021**, *9*, 1606. [CrossRef]
79. Sharifi, H. Analytical Solution for Thermoelastic Stress Wave Propagation in an Orthotropic Hollow Cylinder. *Eur. J. Comput. Mech.* **2022**, *31*, 239–274. [CrossRef]
80. Jing, Y.F.; Huang, T.Z. On a new iterative method for solving linear systems and comparison results. *J. Comput. Appl. Math.* **2008**, *220*, 74–84. [CrossRef]
81. Darvishi, M.T.; Hessari, P. A modified symmetric successive overrelaxation method for augmented systems. *Comput. Math. Appl.* **2011**, *61*, 3128–3135. [CrossRef]

Disclaimer/Publisher's Note: The statements, opinions and data contained in all publications are solely those of the individual author(s) and contributor(s) and not of MDPI and/or the editor(s). MDPI and/or the editor(s) disclaim responsibility for any injury to people or property resulting from any ideas, methods, instructions or products referred to in the content.